

# A proposal of building new muon small wheels : the NSW project

Draft 2.00 18.10.2011 — RPC + MDT

## Abstract

*abstract*

## 1 Introduction [TK]

We propose to build a pair of new small wheel detector (NSW) to replace the existing ones during the second long shutdown<sup>1</sup> of the LHC during which the LHC will be upgraded to achieve its luminosity beyond the nominal design value and up to  $2\text{-}3 \times 10^{34} \text{ cm}^{-2}\text{s}^{-1}$  in the following running period. The goal of NSW is to bring a significant enhancement of the muon performance in the endcap region, in particular of the level-1 muon trigger as well as the precision muon tracking, that would not be achieved by simple and thus lower cost modifications alone such as improvement of radiation shielding, addition of new detector layers or upgrade of electronics.

The muon small wheel is a part of the ATLAS muon spectrometer located in the endcap region in front of the endcap toroidal magnet. This is the innermost station of the three muon stations of the endcap. There are two identical sets of detectors in both sides of ATLAS. The small wheel consists of 4+4 layers of monitored drift tubes (MDT) for precision tracking in the bending direction ( $R$  direction) and two layers of thin gap chambers (TGC) for azimuthal coordinates. These detectors cover the  $\eta$  range of  $1.3 < |\eta| < 2.0$ . The inner part of the small wheel is covered by four layers of cathode readout chambers (CSC) because of its high rate capability. Each CSC layers determines both bending and azimuthal coordinates. The coverage of the CSC chambers is  $2.0 < |\eta| < 2.7$ .

Just to check if reference works [1]. Once more to see the order is OK [2].

## 2 Upgrade motivations [TK]

*Discussion of muon spectrometer performance at high luminosity - precision tracking and L1 trigger, and conclude that new detector and electronics are needed.*

*Point out serious (?) performance degradation in the small wheel region in both MDT and CSC, referring to the radiation background discussoin in Appendix. Performance of the present*

---

<sup>1</sup>Currently it is foreseen in 2018.

detector should be evaluated for high lumi conditin, either using high lumi Monte Carlo or overlay of real events. CSC is 4 layers.

In the L1 discussion, emphasise the importance of maintaining low  $p_T$  threshold. There are two issues. the high rate of fake triggers in the endcap region based mainly on the study using data. Then introduce basic idea of how this can be mitigated by integrating the small wheel in the L1 trigger. As the second point of trigger, discuss the  $p_T$  resolution and possible improvement using the new small wheel. Physics requirement asks low  $p_T$  threshold (20-40 GeV), L1 rate should be maintained at 100 kHz. Need sharpening  $p_T$  threshold. Here introduce 1 mrad requirement.

Finally conclude that NSW should be built and replace the present ones as a phase-1 upgrade item in preparation to running with luminosity beyond the nominal luminosity.

### **3 Requirements for the new small wheel [LP]**

*A short section with short subsections, summarising lists of requirements in numbers.*

#### **3.1 Tracking**

*Segment reconstruction with required performance. Resolution, efficiency, fake, ....*

#### **3.2 L1 trigger**

*Real-time segment reconstruction with required performance. Resolution, efficiency, fakes, ...  
Delay of signal availability.*

#### **3.3 Detector ageing**

*Integrated dose, Detector (and electronics) has to survive, or foresee replacement.*

### **4 General Detector ..... [JD]**

*There are n proposed detector concepts which are discussed in next sections. Here, the following 3 points can be discussed commonly.*

## **4.1 Mechanical structure**

*8+8 large-small layout, total space in z and R. Support structure, accessibility, ..*

## **4.2 Radiation shielding**

*The same as now, or possible improvement of radiation shielding, ..*

## **4.3 Alignment**

*Requirements, target figures, important comments which can be made independent of the detail of detector layout.*

## **4.4 Readout electronics**

*Issues common to all concept. Around ROD.*

## **4.5 DCS, services,**

# 6 Detector concept 2 : Integrated MDT-RPC System

## 6.1 Introduction

The dominant motivation behind the present proposal is to considerably increase the performance and rate capability of the triggering and precision tracking system in the Small Wheel in order to match the higher background levels in the Phase I and II upgrade scenarios of the LHC.

For this purpose, we propose a combination of precision and trigger chambers in a sandwich-like arrangement, a MDT chamber with much improved rate capability enclosed by trigger chambers with considerably higher spatial resolution and rate capability.

The MDT chamber in this concept is made from tubes of half the diameter of the presently used tubes, otherwise operating under the same conditions with respect to gas gain, gas composition and pressure. The reduction of the tube diameter from 30 to 15 mm leads to an increase of the rate capability of the tubes by a factor of seven, sufficient to cope with the level of background hits expected at the SLHC.

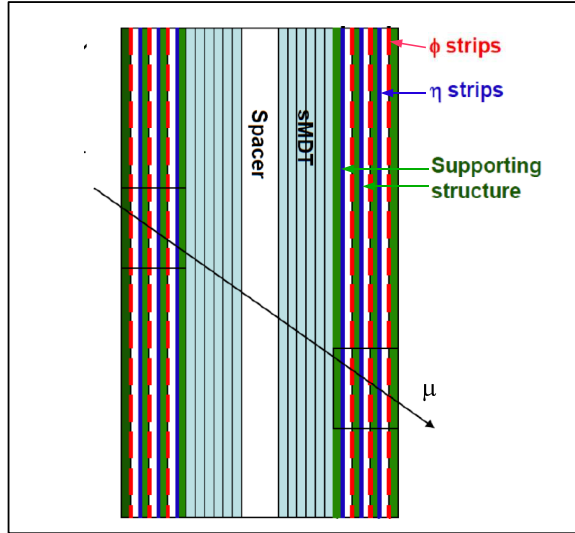


Figure 1: Cross section through the proposed arrangement of trigger RPCs and precision MDTs. The MDT, made out of two multilayers (with 4 or 6 tube layers) is sandwiched between two packages of 3-layer RPCs. The distance of 300 mm between the RPC packages is instrumental for the angular resolution of the triggering muon track.

The RPC trigger chamber will provide considerably improved spatial resolution in the bending plane and at the same time preserve the basic rugged structure and the operating parameters of the proven RPC system, as presently installed in the muon barrel. Due to the reduction of the gap size, ageing will be reduced, while the time resolution will be as good as 2 ns, strongly reducing accidentals from uncorrelated background hits.

The increase of spatial resolution in the RPC trigger chambers is achieved by a much finer granularity of the pickup strips of about 2–3 mm, which is an order of magnitude better than in

the existing chambers, combined with a fast convolution technic, using the induced pulseheights in adjacent strips to deduce the centroid of the avalanche. A spatial resolution of  $<100 \mu m$  can be achieved this way. Tests with particle beams have demonstrated that this level of accuracy can be reached under real experimental conditions, while simulation confirms that the procedure is fast enough to deliver the required information inside the present latency limits and can thus be applied in the phase I of the LHC upgrade.

To distinguish the new trigger chambers, proposed for the New Small Wheel (NSW) from the existing ones in the Big Wheel, we refer to them as to "mRPCs" throughout this article.

In the proposed detector layout, one package of three mRPC chambers is placed in front and one behind the MDT chambers (Fig. 1). A mRPC package will contain three gas gaps, three pickup strips running perpendicular to the radius  $r$  for the  $\eta$ -measurement, the other three radially for the  $\phi$ -measurement. Centroids are centered around local pulseheight maxima on the strips.

One important limitation of the present L1-trigger in the end-cap is due to the fact that a majority of tracks, crossing the Small Wheel, do not originate from the primary vertex and should therefore not be considered candidates for a high- $p_T$  muon by the triggering system. The present trigger, however, can not determine the slope of the candidate track in the  $r$ - $z$  plane and for this reason is unable to discard tracks not coming from the primary vertex. With a distance of about 300 mm between the mRPC packages in front and behind the MDT, an angular resolution of  $\sim 0.4$  mrad (including multiple scattering) can be achieved, which allows to discard tracks not pointing to the primary vertex from the L1 trigger decision. In addition to the precise measurement of the slope in the  $\eta$ -direction, the slope of in the  $\phi$  direction will also be determined, though with less accuracy, to further reduce the number of false triggers. A detailed presentation of the method is given in section 6.2.1.

The limitations of the MDT precision chambers at high luminosity are mainly caused by isolated hits in the tubes ("fake hits"), coming from neutron and gamma conversions in nearby support structures, tube walls, chamber gas and tungsten wires. The presently used 30 mm diameter tubes ("Large tubes") start to lose efficiency if hit rates go beyond about 300 kHz per tube and, therefore, a new MDT chamber type with half the tube diameter is proposed, leading to seven times higher rate capability.

Both new chamber systems, the mRPCs as well as the MDTs, can be operated with the same chamber gas as in the present system. Power requirements for the electronics of both systems will be higher due to higher channel count. Whether this requires active cooling, as is the case for the electronics of the CSC chambers in the region  $\eta > 2$  is under study. Aim is to have services arranged in such a way as to be able to use the existing service infrastructure like e.g. the flexible chains ("cable Schleppts").

### 6.1.1 Upgrade of the RPC System

The basis of the proposed concept is to have as many as possible accurate measurements in the trigger layers, to allow discarding a high percentage of measurements where  $\delta$ -rays, additional  $\gamma$ 's or neutrons are present and still obtain a position measurement from each of the two

packages with a precision of  $\approx 100 \mu\text{m}$ . To obtain such a precision using the 3 mm pitch strips (??) in each gas-gap, while keeping simple electronics, a method using Time-Over-Threshold as an estimate of charge has been developed. The achieved performance using this method for large size mRPCs is discussed in detail in section 6.2.

Achieving this high accuracy for the bending coordinate in each gas volume provides a valuable complement to the MDT position measurements, similar in precision, reducing the required number of tube layers in the MDT necessary for an unambiguous track identification at high background rates. In particular, in the high background rate region of the Small Wheel, having a total of 18 potential measurement points, of which up to 30% may have to be discarded, ensures that an accurate particle vector will be provided in front of the End-Cap Toroidal field, even if some of the layers become non-operational during the exploitation of ATLAS at SLHC. The overall signal processing to produce the trigger is schematically shown in figure ?? of appendix (??).

### 6.1.2 Upgrade of the MDT System

As mentioned in the introduction, the large majority of hits in the Monitored Drift Tube (MDT) chambers are caused by Compton scattering of  $\gamma$ 's which, in turn, come from neutron capture in the material of the chambers and adjacent support material. The resulting hit densities strongly increase towards the inside of the Small Wheel, while, on the other hand, the length of the tubes in the trapezoidal geometry of the SW decreases proportional to the distance from the beam line ( $r$ ). Hit densities, however, are increasing considerably faster than with  $1/r$ , and therefore the highest tube hit rates are at the innermost radii of the chambers.

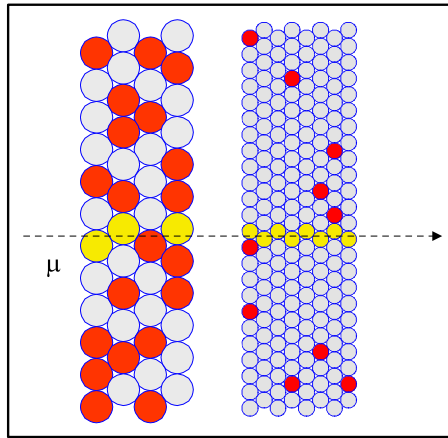


Figure 2: The tracking quality in 30 mm and 15 mm drift tubes in a region of high  $n/\gamma$  background. The occupancies from background hits (red dots) are 50% in the 30 mm tubes but only 7% in the 15 mm tubes due to shorter drift time and smaller area.

Reduction of the drift-tube diameter from 30 mm to 15 mm, while keeping the other parameters unchanged (gas composition and gain, sense wire diameter and tube wall thickness) leads to a significant improvement of the rate capability of the drift-tube chambers, more than sufficient for their operation in the NSW up to the highest background rates expected at 5 times the LHC design luminosity as is illustrated in Fig. 2.

Chamb. type	Tube layers	Location in r	Tube length	Expected hit rate	Count rate per tube	Occupancy	Tube efficiency	Segment efficiency
		<i>cm</i>	<i>cm</i>	<i>Hz/cm<sup>2</sup></i>	<i>kHz</i>	<i>%</i>	<i>%</i>	<i>%</i>
EIL0	2×6	93	56	14000	1176	23,5	79,0	99.8
EIL1	2×4	208	125	5150	965	19,3	82,4	99.9
EIL2	2×4	318	179	1978	530	10,6	90,0	99.9

Table 1: Expected hit rates and efficiencies for 15 mm tubes in a large sector of the NSW. In col. 3 the radial location of the innermost tube of each chamber and in cols. 4 to 8 the tube lengths, the expected hit rates, the counting rates per tube, the occupancies and the  $3\sigma$  single-tube and the track segment reconstruction efficiencies of a chamber are given for the tubes with highest counting rate at a luminosity of  $5 \times$  nominal (times a factor of 2, see text).

Table 1 presents tube hit rates, occupancies and efficiencies for the innermost tubes of the three chambers in a Large Sector of the NSW. Chamber EIL0 covers the area now taken by the CSC. The numbers in col. 4 are based on hit rate measurements at a luminosity of  $9 \cdot 10^{32} \text{ cm}^{-2}\text{s}^{-1}$ , scaled up linearly to  $5 \cdot 10^{34} \text{ cm}^{-2}\text{s}^{-1}$ . Rates in the CSC region ( $1 \text{ m} < r < 2 \text{ m}$ ) are extrapolated from larger radii, using an exponential law [22]. In addition, these rates have been multiplied by a factor of 2 in order to increase rates to the  $14 \text{ kHz/cm}^2$  specification of this Technical Proposal. This factor of 2 could also be considered an additional safety factor in case the real rates will increase faster than predicted by the extrapolation. The efficiencies are calculated from  $\exp(-\tau \cdot f) \approx 1 - \tau \cdot f$ , where  $\tau$  is the dead time after a hit (we use the maximum drift time of 200 ns) and  $f$  the hit rate per tube.

Being able to use the MDT tracking concept at very high background rates allows to preserve the main advantages of the drift tube concept:

- (a) High pattern recognition and tracking efficiency up to high background rates.
- (b) High position and angular resolution, independent of the angle of incidence onto the chamber plane. This property of drift tube chambers with their *circular* drift geometry is a decisive advantage over drift chambers with *rectangular* drift geometry.
- (c) Operational independence of the drift tubes, where a malfunction of any individual tube can only generate a negligible inefficiency.
- (d) Modularity and mechanical robustness of chamber construction.
- (e) Direct connection of the high intrinsic mechanical precision of the chambers to the global optical alignment system.
- (f) Extensive experience in the construction, quality assurance and operation of the MDT chambers in ATLAS; easy integration into the DAQ, trigger and muon reconstruction chains.

For the standard MDT gas mixture of Ar:CO<sub>2</sub> (93:7) at 3 bar absolute pressure, the gas gain of  $2 \cdot 10^4$  is achieved at an operating voltage of 2730 V for 15 mm diameter drift tubes (Table ??). Under these operating conditions, the maximum drift time is reduced by a factor of

3.5 from about 700 ns to 200 ns [14]. In addition, the background flux, hitting a tube of given length is reduced by a factor of two. Altogether, the drift-tube occupancy is thus reduced by a factor of 7. At a background rate of 14 kHz/cm<sup>2</sup>, the expected maximum at the innermost radius at SLHC, the highest occupancy is 23%, corresponding to a counting rate of 1176 kHz (cf. Table 1). The 2×6 drift-tube layers at radii  $R < 2$  m and the 2×4 layers at larger radii provide very robust tracking with track segment reconstruction efficiencies above 99% up to the highest background rates [17]. In this configuration, the point and angular resolution of the drift tube chambers will be uniformly 45  $\mu$ m and 0.5 mrad, respectively, compared to 40  $\mu$ m and 0.45 mrad without background irradiation.

The mechanical structure and the alignment system will be as similar as possible to the ones in the present Small Wheel architecture. Like in the case of the trigger chambers, new readout electronics with higher rate capabilities will have been installed, see section 6.5.

## 6.2 Detector technology and layout

### 6.2.1 Detector technology of the mRPC chambers

### 6.2.2 Detector technology and layout of the sMDT chambers

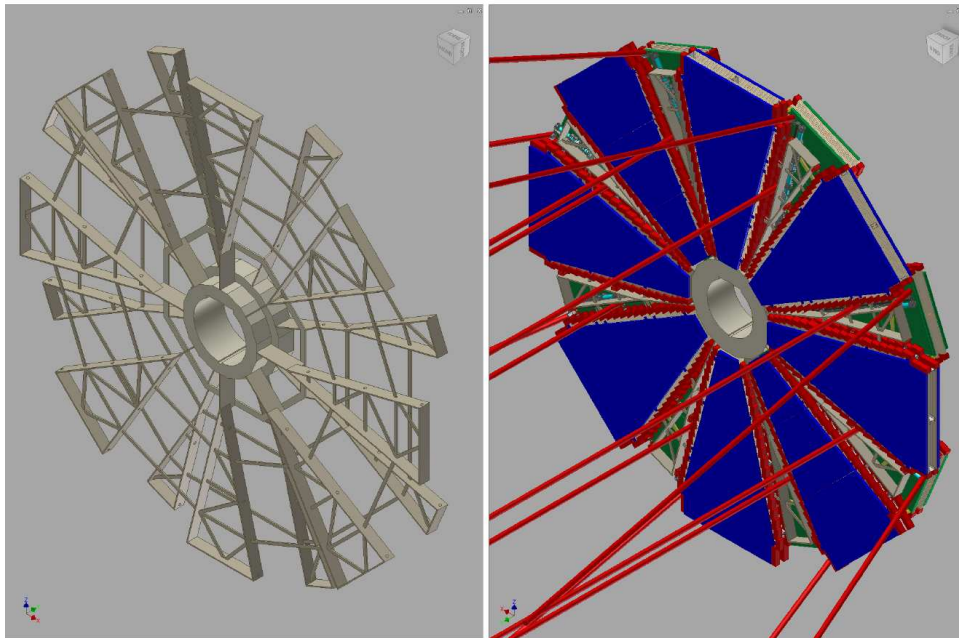


Figure 3: Structure of the NSW (left) and 3D layout of the sMDT-mRPC chamber system (right) with the global alignment rays indicated as red tubes.

The layout of the sMDT chambers for the NSWs follows exactly the present layout of the MDT chambers in the Small Wheels with fully projective small and large chamber towers in combination with the EM and EO layers. (see Figs. 3 and 4). The chamber parameters are summarized in Table 2. There are only three radial chamber segments in each sector. The mRPC chambers are precisely positioned and kinematically mounted on the outer tube layers

of the sMDT chambers on both sides. The integrated sMDT-mRPC chamber packages are connected by light rays to the global optical alignment system and with the neighbouring chambers via sensors mounted precisely on the outer tube layers of the inner multilayers of the sMDT chambers while the in-plane alignment system is integrated into the sMDT spacer structure which also carries the common chamber supports. The well understood alignment system implementation guarantees precise absolute chamber alignment from the beginning which is essential for the performance of the muon spectrometer.

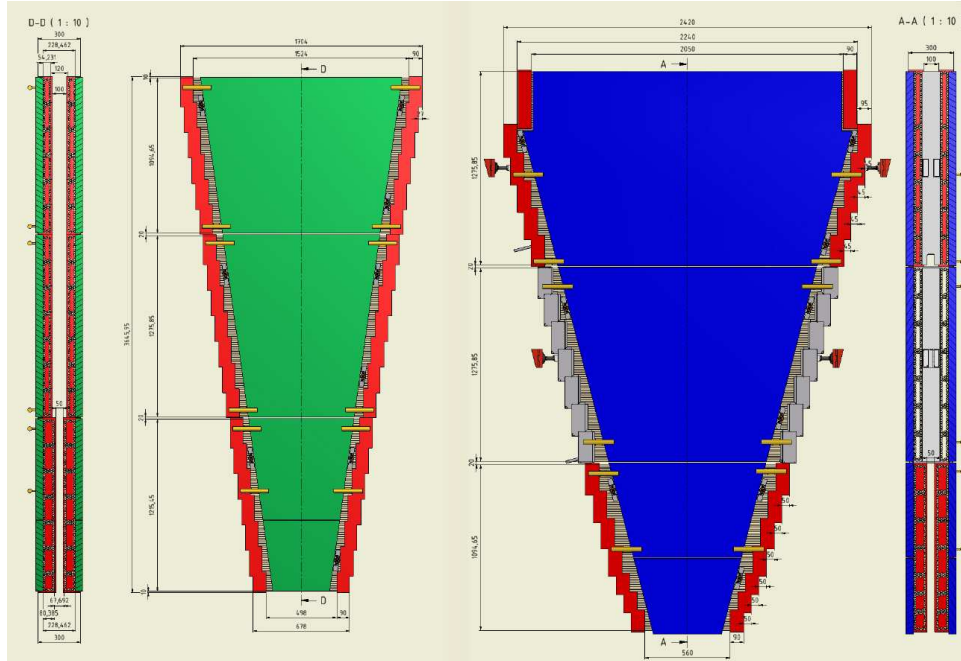


Figure 4: Layout of the integrated sMDT and mRPC chambers in the small (left) and large (right) sectors of the NSW.

The design of the muon drift-tube chambers with 15 mm diameter tubes for the new Small Wheels follows as closely as possible the current ATLAS MDT chamber design in the endcap region of the muon spectrometer (Fig. 5). The chambers consist of two multilayers of four or six layers of drift tubes each in densest package. The aluminum tubes of 15 mm outer diameter and 0.4 mm wall thickness are produced according to industry standard and are chromitized for cleaning and reliable electric contact. The tubes are separated by 0.1 mm wide glue gaps during chamber assembly. The two multilayers are separated by a spacer frame carrying the supports of the integrated drift-tube and trigger chambers on the Small Wheel structure and the in-plane optical alignment system monitoring the planarity of the chambers. The aluminum spacer frame is of similar design as for the present Small Wheel MDT chambers. The main changes in the chamber design are due to the four times denser packaging of the drift tubes and their gas and electrical connections.

Central to the chamber design is the design of the drift tubes and of their endplugs (see Fig. 6). The aluminum tubes have 15 mm outer diameter and 0.4 mm wall thickness and are produced according to industry standards (DIN). The endplugs insulate the sense wire from the tube wall, center the wire in the tubes, position it with respect to the external reference surface on the endplug with an accuracy of only a few micron and provide high-voltage-safe connections to the gas distribution manifold (see Figs. ??) and to the 24-channel readout and

sMDT chambers	EIL0	EIL1	EIL2	EIS0	EIS1	EIS2
Number of chambers	2 x 8	2 x 8	2 x 8	2 x 8	2 x 8	2 x 8
Radial extension (mm)	1095	1095	1457	1215	1276	1095
Minimum chamber width (mm)	740	1428	1968	678	1056	1434
Maximum chamber width (mm)	1380	1878	2418	1002	1380	1704
Minimum tube length (mm)	560	1248	1788	498	876	1254
Maximum tube length (mm)	1200	1698	2238	822	1200	1524
Spacer height (mm)	68	120	120	68	120	120
Thickness in z, tubes (mm)	228	228	228	228	228	228
Thickness in z, chamber (mm)	300	300	300	300	300	300
Weight/chamber (kg)	150	130	180	140	120	130
Number of tube layers	2 x 6	2 x 4	2 x 4	2 x 6	2 x 4	2 x 4
Number of tubes/layer	72	72	96	80	84	72
Number of tubes/chamber	864	576	768	960	672	576
Total number of tubes	13824	9216	12288	15360	10752	9216
Gas volume/chamber (l)	122	162	219	102	110	127

Table 2: Parameters of the sMDT chambers in the NSWs. The total number of drift tubes is 70656 and the total gas volume in each NSW 6750 l.

high-voltage interface boards ("hedgehog cards", Figs. ??).

The modular gas distribution system consists of injection moulded plastic tubes made of Pocan<sup>®</sup> without glass fiber which interconnect adjacent tubes in the direction perpendicular to the multilayer and connect them to an aluminum gas distribution bar on the readout and the high-voltage end of the multilayer.

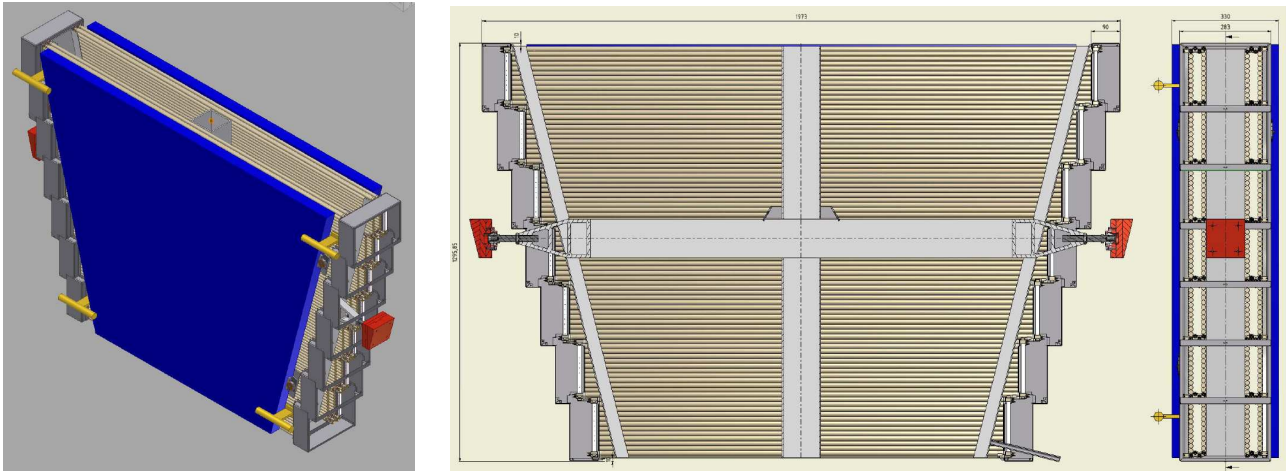


Figure 5: Small drift-tube chamber design for the new Small Wheels: 3D view (left) and cross sections in the chamber middle planes parallel and perpendicular to the tube layers (right). The mounting of the trigger chambers and of the external alignment sensor is also shown.

The readout and high-voltage supply scheme follows closely the one of the present MDT chambers using the same parameters and specifications. The high-voltage decoupling capacitors on the readout side and the terminating resistors on the high-voltage supply end are individually encapsulated in plastic containers for high-voltage protection. The plastic containers are

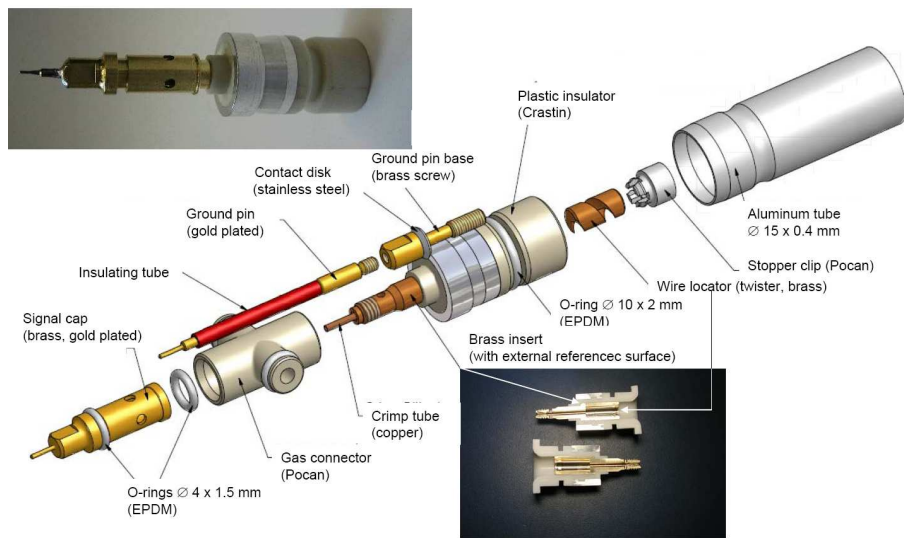


Figure 6: Exploded view of a drift tube with gas, signal and ground connections.

integrated with the hedgehog cards plugged onto the gold-plated pins of the signal caps and ground connectors. The ground pins are screwed into the gaps formed by three adjacent tubes. In order to during chamber assembly to connect the tube walls to the ground of the hedgehog cards. This scheme allows for the high-voltage-free design of the readout hedgehog cards. Each readout hedgehog card carries a mezzanine card with the new radiation hard active readout electronics (see below). The mezzanine cards follow the shape of the hedgehog cards and are currently under development. The electronics boards are enclosed in aluminum Faraday cages which also shield the readout hedgehog cards against the mezzanine cards. The modularity of the sMDT chambers in the NSW is given in Table 3.

## 6.3 Performance

*Summary of chamber performance, details in appendix of technology.*

*Spatial and angular resolution as functions of rate and angle of incidence*

*Time resolution*

*Efficiency (single measurement and segment)*

*Double track resolution*

*Rejection of fake and background tracks*

### 6.3.1 Performance of the RPC trigger chambers

The most important issue for a detector that needs to operate at high rate during a period of more than 10 years, is its aging characteristics. For this reason, a small RPCs ( $xx \times yy \text{ cm}^2$ ) detectors were constructed and exposed to  $\gamma$  irradiation for various periods of time. No deterioration was observed in any of these prototypes.

### 6.3.2 Performance of the sMDT tracking chambers

In order to verify the performance of the 15 mm diameter ("small") drift tube chambers, extensive tests of the full-scale prototype chamber with 15 mm diameter drift tubes have been performed in the H8 high-energy muon beam in 2010 and 2011 together with RPC chambers (see Fig. ??, left) and, using cosmic ray muon tracks, in the CERN Gamma Irradiation Facility (GIF) with a 500 GBq  $^{137}\text{Cs}$  source (Fig. ??, right). The standard ATLAS MDT readout electronics has been used with the adjustable deadtime set to the minimum value corresponding to an overall effective deadtime of 200 ns. The spatial resolution and efficiency of the individual drift tubes and of the whole chamber have been measured for different  $\gamma$  irradiation rates where the individual drift tubes have been illuminated uniformly over the whole length.

As a measure for evaluating the tracking efficiency, we define the "3 $\sigma$ -efficiency" as the probability of detecting a tube hit within a distance of 3 times the drift tube resolution  $\sigma$  from the muon track, the muon track being defined by the other tubes on the track, extrapolated to the active volume of the tube. Similarly, the drift tube resolution as a function of the drift radius is determined by an iterative method excluding the evaluated tube from the track reconstruction in the chamber [21].

Fig. 7 shows the average 3- $\sigma$  efficiency of 15 mm diameter drift tubes and the track segment reconstruction efficiency of the prototype chamber as a function of the  $\gamma$  background flux in comparison with the results for the 30 mm diameter tubes from previous tests of a BOS MDT chamber in GIF [12], [13]. At low background rate, the 3 $\sigma$  tube efficiencies of 30 and 15 mm diameter tubes are 94% and 96%, respectively. The efficiency loss is due to  $\delta$ -rays created by interaction of the muons with the tube walls which produce hits earlier than the muons. The degradation of the efficiency with increasing rate follows the predicted behaviour. The

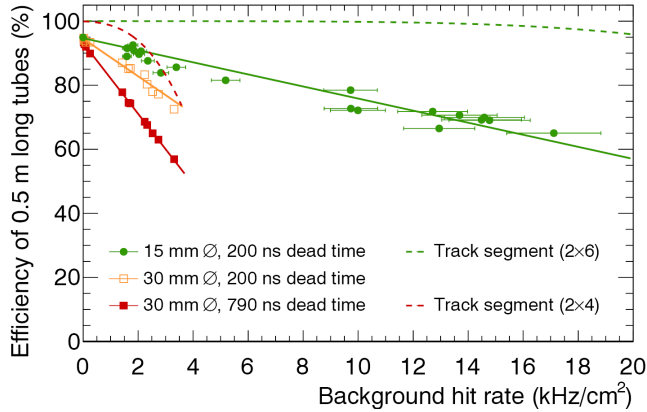


Figure 7: The  $3\sigma$  efficiency of individual drift tubes as a function of the background hit rate as measured at the GIF. Results for 15 mm and 30 mm diameter tubes are compared. The corresponding track segment reconstruction efficiencies in 2 x 4 layer MDT chambers and 2 x 6 layer sMDT chambers are indicated as dashed curves and have been calculated from the tube efficiencies requiring at least two hits in each multilayer.

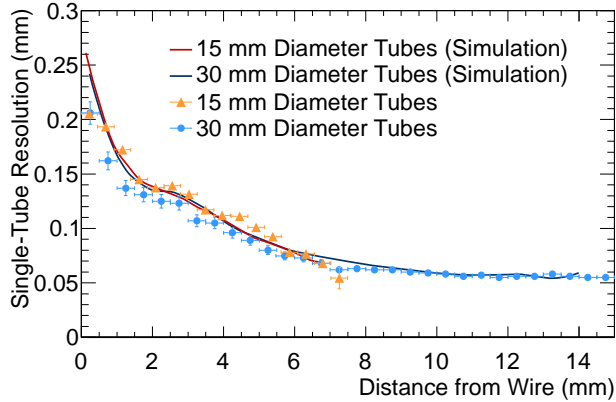


Figure 8: Spatial resolution of large and small tubes in the H8 test beam together with simulation results.

redundancy of track measurements in the different drift tube layers is sufficient to achieve almost 100% track segment reconstruction efficiency up to the highest background rates.

In Fig. 8 the spatial resolutions of 15 mm and 30 mm diameter drift tubes measured without background irradiation in the high-energy muon beams H8 and X5, respectively, at CERN as a function of the drift radius  $r$ . The latter is determined using an external reference, the other drift tube layers of the prototype chamber in the H8 beam vs. a silicon strip detector beam telescope in the X5 beam. The radial dependence of the 15 mm diameter tube resolution agrees with the 30 mm diameter tube resolution measurement for  $r < 7.5$  mm as expected. The average resolutions including time-slewing corrections of 15 and 30 mm diameter tubes at low background rates are  $110 \pm 10 \mu\text{m}$  and  $80 \pm 5 \mu\text{m}$ , respectively.

## 6.4 mRPC Level-1 trigger and readout electronics

The strip signals in the mRPC of the NSW are used to extrapolate tracks to the Big Wheel where they are corroborated by the Sector Logic with the existing 2-out-of-3 and 3-out-of-4 coincidences in the Big Wheel chambers. The fine granularity of the extrapolation results in high efficiency for trigger rejection. The electronics added to accomplish this must not cause the latency to the Sector Logic to exceed the existing  $1.05\ \mu\text{s}$ . A detailed breakdown of the mRPC trigger latency is given in the appendix (??).

## 6.5 Readout Electronics of the sMDT Chambers

The readout of the Small MDT tubes will follow the proven architecture of the present MDT system. A number of additions and modifications, however, will be necessary in order to adapt the rate capability of the readout chain to the requirements of the SLHC. For the mechanical integration of the readout electronics with the Small tube chambers, the layout of the electronics will have to be adapted to the four times higher tube density at the ends of the chambers. Finally, the radiation tolerance of all components will have to comply with the high radiation levels, in particular at the inner boundary of the Small Wheel.

### 6.5.1 Architecture of the present MDT chamber readout

In the present readout scheme tube signals are routed via a PCB ("hedgehog card") to a piggy-back card ("mezzanine card"), containing an Amplifier and Shaper, followed by a Discriminator with adjustable threshold, all three functions being integrated in a radiation tolerant ASIC (ASD). The discriminator outputs, in turn, are routed to a TDC, where each leading and trailing edge signal receives a high-precision time stamp, which is retained, together with the corresponding channel number, in a large internal buffer of the TDC ("Level-1 buffer").

When the TDC receives a Level-1 trigger, a subset of the recorded hits, corresponding to a pre-defined time window, are retained for readout and are forwarded to the data concentrator of this chamber, the "Chamber Service Module" (CSM). From there, data are sent to the off-chamber electronics in USA15, the "Readout Driver" (ROD). A CSM can serve up to 18 mezzanine cards. The operation parameters of the analog frontend (ASD) and the TDC are controlled by a JTAG string, which is distributed by the Detector Control System (DCS) to the CSM, which sends it individually to each mezzanine card. Fig. 9 gives the layout of the present system. A detailed presentation of the MDT readout electronics is given in [5]. The ASD and TDC ASICs are described in [7] and [8].

### 6.5.2 Architecture of the sMDT chamber readout

For the evolution of this architecture into matching the requirements of the Small tube readout, a number of problems limiting the performance of the present scheme has to be overcome. Given the high rate capability of the Small MDT tubes, the bandwidth of the readout system has

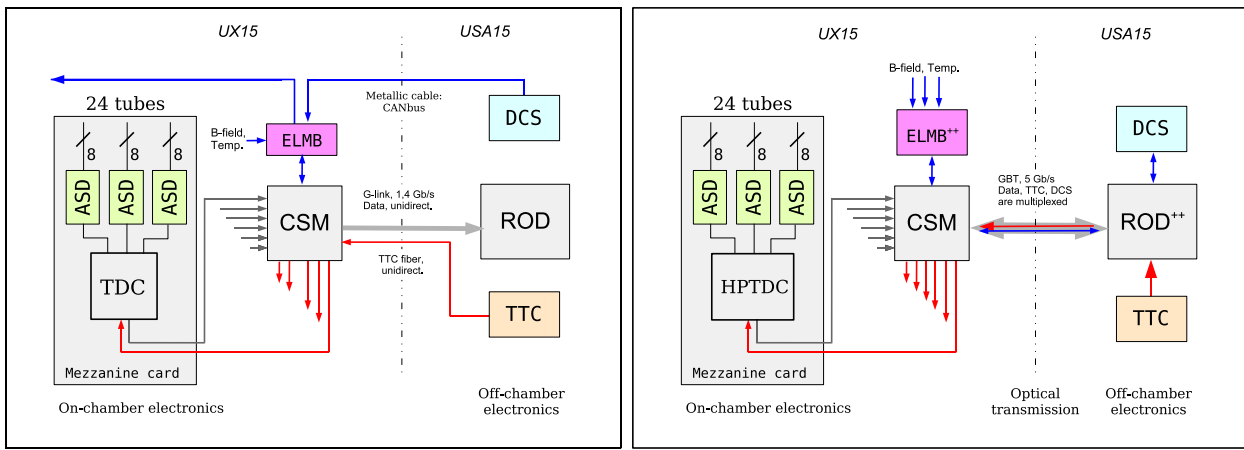


Figure 9: Schematic diagram of the present (left) and of the future MDT readout chain (right). Using the GBT in the new readout scheme improves the readout bandwidth and simplifies logistics, as TTC, Data readout and DCS are transferred over the same bi-directional link. The omission of CANbus cabling due to GBT will reduce the risk of ground loops between chambers and improve system reliability.

to be increased. Due to the limitations of the internal buffering scheme and processing speed, the present TDC can only handle average tube rates up to about 300 kHz per tube without losing data, while tubes in the NSW would run up to 1200 kHz (Table 1). An improved TDC is therefore an essential requirement for a new readout design.

Another limitation of the readout bandwidth comes from the optical link, connecting the CSM to the ROD, which only provides a usable bandwidth of 1,4 Gbit/s. Fig. 10 shows occupancy and efficiency of Large and Small tubes as a function of tube hit rate.

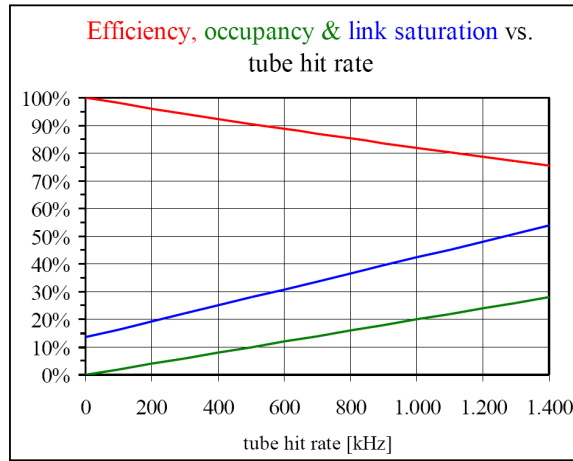


Figure 10: Green: Occupancy as a function of tube hit rate, assuming a dead time of 200 ns (equal to the maximum drift time) after each hit. Red: Resulting efficiency with 200 ns dead time. Blue: Saturation of the mezzanine-to-CSM link at 100 kHz L1 trigger rate. The load of 15% at zero hit rate is due to overheads in the transfer protocol.

The technologies used for the existing ASICs in the MDT readout are no more available from industry, and the following new components have therefore to be introduced into the new

readout system.

- (a) The ASD is re-designed in the IBM 130 nm technology. A 4-channel prototype, demonstrating the analog parameters, has already been produced and works correctly. Most analog parameters of the previous design are preserved. A full 4-channel prototype chip including the digital part (see Fig. 11) has been delivered in September 2011 and is under test. The final step in the ASD chip design is the extension to 8 channels.
- (b) The TDC will be replaced by the HPTDC, designed by the CERN-MIC group ([6]). This 32-channel device has an improved internal buffering scheme as well as higher transfer and processing speeds. If only 24 out of the available 32 channels are used, the unused channels can be disabled to save power.
- (c) The CSM collects data from a MDT chamber, formats the event and sends data, trigger-by-trigger, via an optical link to the ROD in USA15. All logical operations are performed by an FPGA, which will need to be upgraded to higher radiation tolerance. While the present CSM serves up to 18 mezzanine cards, the new CSM will have to serve up to 24 cards.
- (d) The link connecting the CSM to the ROD will be replaced by a GigaBit Transmitter link (GBT), developed by CERN. This link provides a 3 times higher transfer rate (Gbit/s), compared to the presently used S-link [9].
- (d) The readout of voltages and temperatures on the mezzanine cards will be done via the DCS channel of the GBT. To collect ADC readings from temperature sensors on the chamber and from B-field probes, a new version of the ELMB will be used. Aim would be to interface this new device ("ELMB++") directly to the CSM, so these data could be read out through the DCS channel of the GBT. This way, the presently used CANbus cabling could be omitted, simplifying installation and reducing the risk of ground loops.



Figure 11: The new 4-channel ASD chip with full analog and digital functionality on the test board.

Another stringent requirement for the realization of the new readout scheme is the mechanical integration of the on-chamber readout electronics with the chamber mechanics, as the

Chamb. type	Tubes $\times$ layers $\times$ MLs	Tubes/chamber	Tubes total	Mezz.cards/chamber	Mezz.cards total	CSMs/chamber	CSMs total
EIL0	$72 \times 6 \times 2$	864	13824	36	576	2	32
EIL1	$72 \times 4 \times 2$	576	9216	24	384	1	16
EIL2	$96 \times 4 \times 2$	768	12288	32	512	2	32
EIS0	$80 \times 6 \times 2$	960	15360	40	640	2	32
EIS1	$84 \times 4 \times 2$	672	10752	28	448	2	32
EIS2	$72 \times 4 \times 2$	576	9216	24	384	1	16
Total side A + C:			70656		2944		160

Table 3: Electronics channels (drift tubes) and readout boards in the NSW. Each mezzanine card serves 24 drift tubes, matching the modularity of the chambers with 6 and 4 tube layers per multilayer. Each CSM serves up to 24 mezzanine cards. Chambers with more than 24 mezzanine cards are served by two CSMs.

density of channels at the tube ends is four times higher than in the case of the 30 mm tubes. The following design changes will therefore be implemented.

- (a) HV decoupling capacitors are located in 15 mm diameter cylinders at the tube ends, see Fig. ???. The density of signal routing on hedgehog cards is thus no longer limited by insulation distances between HV and ground or signal traces on the PCB.
- (b) To match the higher tube density, the space on the mezzanine card has to be used more efficiently. For this purpose, the passive protection circuitry of the ASD inputs will be moved to the hedgehog card.
- (c) For the interconnection between mezzanine cards and new CSM, we foresee to use the same 40-wire cables as was used in the present system. Its moderate diameter and high flexibility may be important for fitting the new MDTs into the limited space in the Small Wheel.

The modularity of the readout system of the Small tube sMDTs for the NSW is given in tab. 3.

### Power consumption of the electronics

While the power consumption of the on-chamber frontend electronics of the present system is about 30–40 W/chamber ([5], table 3), the consumption will now be about 2.5 times as high, due to tube density and increased consumption of TDC, optical link and other component.

A detailed breakdown of the expected power consumption of the MDT chambers in the NSW is presented in Table 4. The total power consumption of 8.4 kW is less than the consumption of the presently installed CSC (11.5 kW, see [2], Table 46). Yet, the removal of the heat may require flushing with dry air, as significant temperature gradients may influence the spatial resolution of the MDT and natural air convection is obstructed by the tight space constraints in the high- $\eta$  region of the Small Wheel.

Chamber type	mezz.s/ chamber	current/ mezzan.	current/ CSM	current/ chamber	power/ chamber at 3.3 V	power/ chamber at 4.5 V
		<i>A</i>	<i>A</i>	<i>A</i>	<i>W</i>	<i>W</i>
EIL0	36	18	3	21	69.3	94,5
EIL1	24	12	1.5	14	44.6	60.8
EIL2	32	16	3	19	62.7	85,5
EIS0	40	20	3	23	75.9	103.5
EIS1	28	14	3	17	56.1	76.5
EIS2	24	12	1.5	14	44.6	60.8
Power per Large + Small sector [W]					353	482
Power per side [W]					2825	3852

Table 4: Power requirements for the readout electronics of the NSW. Each mezzanine card consumes about 0.5 A, each CSM about 1.5 A at 3.3 V. The voltage delivered to the CSM is assumed to be 4.5 V, the voltage difference being consumed in local voltage regulators.

## 6.6 L1 trigger and electronics

1. *How the L1 signal are produced, starting from the detector signal till the formation of SL input.*
2. *Latency (calculation, measurement with demonstrator)*
3. *Compatibility with Phase II upgrade*

## 6.7 Readout electronics and integration in DAQ

1. *Detailed description of electronics chain*
2. *Integration to DAQ*
3. *Readout related parameters, e.g. bandwidth requirements, number and granularity of read-out links*
4. *Compatibility with Phase II upgrade*

## 6.8 Services, infrastructure and DCS

1. *Description of service scheme (including power system, read-out, trigger, alignment), cooling needs and other special requirements*
2. *Table with number of services (number of cables, outer diameter, cross section of leads)*
3. *Table with power consumption (per channel, chamber, total)*
4. *Required rack space*

Cable	Number of cables (granularity)	Outer cable diam. (mm)	Cross section of leads (mm <sup>2</sup> )
HV			
LV			
Monitoring and control			
Front-end links			
Calibration			
Alignment			
Miscellaneous			

Table 5: Example table number of services per chamber

Chamber	Number of channels	Power consumption per channel	Total power consumption
---------	--------------------	-------------------------------	-------------------------

Table 6: Example table: Number and types of chambers per sector

(a) UX15 (include maximum allowed distance to detector if any)

(b) US15 (power system)

(c) USA15 (DAQ)

5. Gas system and distribution

*Details on number of gas manifolds per sector (include drawings) and connections to chambers (serial, parallel?). Size of pipes*

*Required nominal, minimum, and maximum flow*

*Required precision of gas mixture*

*Safety measures in case of inflammable gas*

*Required rack space for gas system in SGX1, USA15, UX15*

6. Integration in DCS system, requirements for DCS

## **7 Expected muon performance with NSW [sv]**

*Discussion of overall performance. L1 trigger, muon reconstruction, efficiency, fake, sensitivity to a few layout parameters (number of layers, ...),*

## **8 Integration, assembly and commissioning [JD]**

## **9 Cost, resources and schedule [LP, TK]**

## **10 Conclusions**

# Appendices

## A Radiation background

*Discussion of expected cavern background and its uncertainty based on simulations and measurements with muon detectors, and finally give a reference figures and safety factor.*

- *Overview of cavern background. It's nature, origin, shielding strategy*
- *Simulation result. R distribution in the small wheel region. 14 TeV, Al beam pipe, 14 TeV steel beam pipe, 7 TeV steel beam pipe.*
- *Measurements with pp collision. MDT, CSC*
- *Summary figure. Reference figures.*

### A.1 simulation



# References

- [1] G. Aad et al. Expected Performance of the ATLAS Experiment - Detector, Trigger and Physics. 2009.
- [2] G. Aad et al. The ATLAS Experiment at the CERN Large Hadron Collider. *JINST*, **3** S08003 (2008)
- [3] M. Bosman et al. Estimation of Radiation Background, Impact on Detectors, Activation and Shielding Optimization in ATLAS, ATLAS Note *ATL-GEN-2005-001* (2005)
- [4] P. Barrow, G. Conti, M. Franklin and L. Jeanty, Cavern Background, Muon Upgrade meeting, july, 29th, 2011 <https://indico.cern.ch/conferenceDisplay.py?confId=148910>
- [5] Y. Arai et al., ATLAS Muon Drift Tube Electronics, *JINST* **3** P09001 (2008)
- [6] J. Christiansen et al., Manual and User Application Notes for the HPTDC, (2004), [http://tdc.web.cern.ch/tdc/hptdc/docs/hptdc\\_manual\\_vs2.2.pdf](http://tdc.web.cern.ch/tdc/hptdc/docs/hptdc_manual_vs2.2.pdf) and <http://tdc.web.cern.ch/tdc/hptdc/hptdc.htm>
- [7] Posch C., Hazen E., Oliver J., MDT-ASD User's Manual, (2007), ATL-MUON-2002-003; [https://edms.cern.ch/document/899037/2/ASD\\_Manual\\_vs\\_2007.pdf](https://edms.cern.ch/document/899037/2/ASD_Manual_vs_2007.pdf)
- [8] Y. Arai, AMT-3 User Manual, [https://edms.cern.ch/file/897562/1/AMT3manual\\_033.pdf](https://edms.cern.ch/file/897562/1/AMT3manual_033.pdf), [http://atlas.kek.jp/tdc/amt3/AMT3manual\\_033.pdf](http://atlas.kek.jp/tdc/amt3/AMT3manual_033.pdf)
- [9] P. Moreira, find some reference to the GBT!!
- [10] M. Deile et al., *Performance of the ATLAS Precision Muon Chambers under LHC Operating Conditions*, Proceedings of the 9<sup>th</sup> Pisa Meeting on Advanced Detectors, Isola d'Elba, Italy, 25–31 May 2003, Nucl. Instr. and Methods **A518** (2004) 65;  
M. Deile et al., *Resolution and Efficiency of the ATLAS Muon Drift-Tube Chambers at High Background Rates*, Proceedings of the 10<sup>th</sup> Vienna Conference on Instrumentation, Vienna, Austria, 16–21 February 2004, Nucl. Instr. and Methods **A535** (2004) 212;  
S. Horvat et al., *Operation of the ATLAS Muon Drift-Tube Chambers at High Background Rates and in Magnetic Fields*, IEEE Transactions on Nuclear Science, Vol. 53, No. 2 (2006) 562.
- [11] J. Dubbert et al., *Development of Precision Drift Tube Detectors for the Very High Background Rates at the Super-LHC*, Proceedings of the 2007 IEEE Nuclear Science Symposium, Honolulu, Hawaii, USA, 28 October–2 November 2007; MPI report, MPP-2007-172, November 2007.
- [12] M. Deile *et al.*, *Performance of the ATLAS Precision Muon Chambers under LHC Operating Conditions*, Nucl. Instr. and Meth. **A 518** (2004) 65; M. Deile *et al.*, *Resolution and Efficiency of the ATLAS Muon Drift-Tube Chambers at High Background Rates*, Nucl. Instr. and Meth. **A535** (2004) 212.
- [13] S. Horvat *et al.*, *Operation of the ATLAS Precision Muon Drift-Tube Chambers at High Background Rates and in Magnetic Fields*, IEEE trans. on Nucl. Science Instr. Vol. 53, 2 (2006) 562.

- [14] B. Bittner *et al.*, *Development of Muon Drift-Tube Detectors for High-Luminosity Upgrades of the Large Hadron Collider*, Nucl. Instr. and Meth. **A617** (2010) 169.
- [15] R. Veenhof, *GARFIELD: Simulation of Gaseous Detectors, Version 8.01*, CERN, write-up: <http://wwwinfo.cern.ch/writeup/garfield>.
- [16] W. Riegler, *High Accuracy Wire Chambers*, Nucl. Instr. and Meth. **A 494** (2002) 173.
- [17] B. Bittner *et al.*, *Development of Fast High-Resolution Muon Drift-Tube Detectors for High Counting Rates*, Nucl. Instr. and Meth. **A 628** (2011) 154.
- [18] M. Aleksa *et al.*, *Rate Effects in High-Resolution Drift Chambers*, Nucl. Instr. and Meth. **A 446** (2000) 435.
- [19] O. Kortner *at al.*, *Alignment of the ATLAS Muon Spectrometer with Tracks and Muon Identification at High Background Rates*, Nucl. Instr. and Meth. **A581** (2007) 545-548.
- [20] H. Kroha, *Quality Assurance and Quality Control Reference Document for ATLAS MDT Chamber Construction*, ATLAS Note, ATL-MUON-2000-008, May 1999.
- [21] S. Horvat, O. Kortner, H. Kroha, *Determination of the Spatial Drift-Tube Resolution Using Muon Tracks*, ATLAS Note, ATL-MUON-PUB-2006-008, July 2006.
- [22] G. Conti, P. Barrow, M. Franklin and L. Jeanty, *Cavern Background Studies from MDT*, <https://indico.cern.ch/getFile.py/access?contribId=2&resId=0&materialId=slides&confId=151320>